

# DEVELOPMENT AND TESTING OF AN INTEGRATED NAVIGATION SENSOR FOR PLANETARY HOPPER NAVIGATION

Ted J. Steiner<sup>1</sup>, Scott A. Rasmussen<sup>2</sup>, Paul A. DeBitetto<sup>3</sup>, and Jeffrey A. Hoffman<sup>4</sup>

<sup>1</sup>*Massachusetts Institute of Technology, 77 Massachusetts Avenue, Cambridge, MA 02139, United States, Email: tsteiner@mit.edu*

<sup>2</sup>*Draper Laboratory, 555 Technology Square, Cambridge, MA 02139, United States, Email: srasmussen@draper.com*

<sup>3</sup>*Draper Laboratory, 555 Technology Square, Cambridge, MA 02139, United States, Email: pdebitetto@draper.com*

<sup>4</sup>*Massachusetts Institute of Technology, 77 Massachusetts Avenue, Cambridge, MA 02139, United States, Email: jhoffma1@mit.edu*

## ABSTRACT

In recent years, considerable attention has been paid to planetary hoppers for their potential to overcome the limitations on landing precision and mobility facing current planetary surface exploration technologies. This paper describes the development of a unified vision and inertial navigation system for propulsive planetary hoppers and provides demonstration of this technology. A sensor testbed, including a stereo vision package and inertial measurement unit, was developed to act as a proof-of-concept for this navigation system architecture. The system is shown to be capable of outputting an accurate navigation state estimate for motions and trajectories similar to those of planetary hoppers.

## 1. INTRODUCTION

Planetary hoppers are vehicles that traverse planetary surfaces using chemical exhaust propulsion alone, freeing them from many of the limitations of rovers and stationary landers. This allows hoppers to fine-tune their landing sites to very high levels of precision, while also allowing exploration of a wide range of otherwise inaccessible terrain. For this reason, analogies such as “reusable landers” and “airless helicopters” are sometimes used to describe the unique mission profiles they enable.

Hopping vehicles provide advantages over traditional surface exploration vehicles, such as wheeled rovers, by enabling in-situ measurements in otherwise inaccessible terrain [1]. However, significant development over previously demonstrated vehicle navigation technologies is required to accommodate the additional, unique motions of hoppers that must be accounted for beyond those typical of conventional planetary landing and surface navigation systems [2]. An example of a conceptual hopper is shown in Fig. 1.

Hopping requires a fully autonomous, internal navigation system capable of handling rapid, near-surface motions in an unknown environment. Autonomy is required due to the long communication delays to the Moon or other



Fig. 1: A conceptual hopper designed for use on the moon. Image credit: Draper Laboratory/Next Giant Leap

planets, which eliminate the possibility of remote operation due to the rapidity of hopper motions. The system must be entirely internal and self-contained because installing a large-scale external navigation system (e.g., a GPS-like system) on another planetary body is prohibitively expensive. The system must be capable of navigating in an unknown environment, as a hopper might be called upon to explore areas unavailable from orbital imagery, such as permanently shadowed craters or underneath overhangs of cliffs [3].

The navigation systems developed for traditional exploration vehicles cannot meet these needs. Navigation systems onboard prototype hoppers currently in development for testing on Earth are typically dependent on either an external system, such as GPS [4], or prior knowledge of their environment [5]. Terminal-descent and landing navigation systems, such as [6–9], are not designed for extensive near-surface operation or high-rate translational motion. Helicopter navigation systems, such as [10–13], are capable of handling translational motion, but are generally dependent on GPS or other external systems, such as a barometric altimeter or remote operator.

## 2. UNIFIED NAVIGATION SYSTEM

Inertial and stereo vision navigation systems were combined using an Extended Kalman Filter (EKF) to form a single, unified inertial and vision-based navigation system. Inertial navigation systems work well for high-rate, short-period motion, and are independent of their operational environments. However, low-cost and mass inertial measurement units (IMUs) have limited capability to precisely measure low-rate, long-period motion due to sensor drift over time.

Vision navigation systems work well for low-rate, long-period motions, but poorly for measuring rapid rotations. Performance of vision systems is also dependent on characteristics of their operational environments, such as lighting conditions, which cannot always be ensured [2]. The unified system, which combines the previously developed inertial and stereo vision navigation systems described below, exceeds the navigation performance of either system taken independently and allows the use of lower cost and mass sensors [3].

### 2.1. Inertial Navigation

The available Inertial Navigation System (INS), developed by Draper Laboratory, combined a low-grade IMU with a GPS receiver, in a similar fashion to those described in the literature [14,15]. Taken alone, the IMU accrues error exponentially with time (a characteristic common to any IMU), so absolute position updates from the GPS receiver were used to frequently constrain this error growth using an EKF. IMUs are well suited to measurement of high-rate, short-period motion, but the integrity of the INS is rapidly lost when GPS updates become unavailable [2].

### 2.2. Vision Navigation

The available vision navigation system was the Draper Laboratory's stereo vision-based Simultaneous Localization and Mapping (SLAM) implementation, hereafter referred to as 'DSLAM,' similar to those in the literature [16]. The basic concept of DSLAM is that a map of an unknown environment is built from observed 3-dimensional "landmarks," whose locations are determined from 2-dimensional "features" detected in pairs of stereo images, and the observer is localized within this map. DSLAM acquires images from a stereo camera and then performs the following steps to determine the position of the camera relative to its initial position: feature detection, feature matching, pose estimation, and landmark registration [3].

## 3. TEST HARDWARE

A sensor testbed, including a stereo vision camera, inertial measurement unit, and GPS receiver, was developed

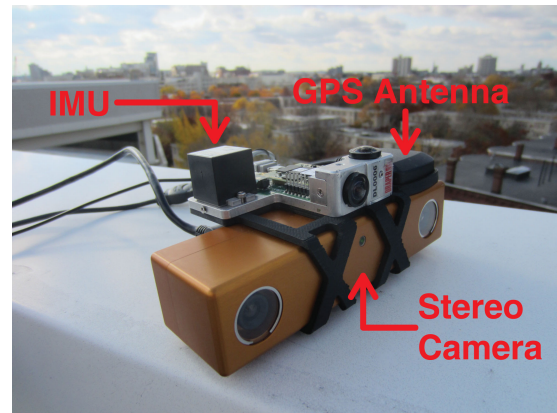


Fig. 2: The Stingray testbed includes a stereo camera, IMU, and GPS antenna. The IMU is accessed using a dedicated interface board that also houses additional, unused sensors.

to allow evaluation of various combinations of navigation sensors and algorithms [3]. This hardware and software testbed, called "Stingray," has a highly modular architecture, allowing additional sensors to be easily added to the system for real-time logging and incorporation into navigation algorithms. The algorithms themselves are fully encapsulated within the software framework, allowing multiple algorithms to run simultaneously for real-time performance comparison. Stingray, shown in Fig. 2, is capable of operating independently of any particular carrier vehicle, allowing it to be tested onboard various flight vehicles with little or no modification required.

### 3.1. Computer

At the core of the Stingray system is a Jetway NF81 single-board computer. The NF81 is a mini-ITX form-factor (17 x 17 cm) motherboard with an AMD Brazos eOntario G-Series APU (combined CPU and GPU). It has 8 GB of DDR3 RAM and an 80 GB mSATA solid state drive (SSD). The system also has a wide range of I/O, including eight USB ports, two RJ-45 (Ethernet) ports, and ten pins of GPIO. A Firewire adapter on a mini-PCIe slot adds an additional three IEEE 1394 Firewire ports.

The Stingray computer runs Ubuntu Linux 11.04 Server Edition, but the software framework is cross-platform compatible, allowing the code to also run on Windows or Mac OS. The computer itself is far more powerful than a typical, space-rated flight vehicle would likely use, ideally allowing multiple navigation algorithms to run in parallel simultaneously for comparison.

### 3.2. Inertial Measurement Unit

The IMU currently in use on the system is an Analog Devices ADIS16364BMLZ industrial-grade MEMS IMU.

A Draper-developed interfacing board, including a digital signal processor (DSP), provides a convenient interface to the IMU, as well as a magnetometer, barometer, and additional cameras, though they are currently unused for this project. The DSP provides precise timestamping of the IMU data, and is capable of precisely recording an external input pulse from the stereo camera.

### 3.3. Stereo Camera

The stereo camera is a BumbleBee2 monochromatic stereo vision camera from Point Grey Research (model BB2-08S2M-6) with 6 mm focal length lenses (43 degree field of view) and frame rate of 20 fps. The camera resolution is downscaled to 512 x 384 pixels for each camera prior to image processing. The camera outputs a strobe pulse to the IMU interface board at the start of integration of each camera frame, which increases timing accuracy by over three orders of magnitude compared to using the primary IEEE-1394a interface for timing purposes.

### 3.4. GPS Receiver

GPS data is provided by a uBlox EVK-6T Precision Timing Kit and ANN-MS-0-005 active GPS antenna, which is capable of outputting GPS position and velocity estimates as well as raw pseudorange data. GPS positioning data is typically accurate to within 2-3 meters and is logged by the main computer over a USB connection at approximately 1 Hz. Although GPS data is not available to planetary hoppers, it is used during testing to provide both an initial position for each dataset and an absolute reference to compare against.

## 4. ADVANTAGES OF THE UNIFIED NAVIGATION SYSTEM

The unified inertial and vision navigation system offers many advantages over the individual systems by reducing IMU drift, improving IMU bias estimation, handling rapid rotations, and managing periods of sensor outages. Fig. 3 and Fig. 4 show a performance comparison of the individual and unified navigation systems for a trajectory involving a straight line and two 90-degree corners, respectively.

### 4.1. IMU Drift

Due to numerical integration of sensor noise, IMU drift error grows exponentially with time until constrained by an external sensor update. Despite growing increasingly erroneous, IMUs have very low drift for brief periods immediately following updates. An IMU receiving frequent updates is capable of providing accurate measurements over a wide range of rotational rates and accelerations. DSLAM can provide these updates more frequently (based on the frame rate of the camera) than

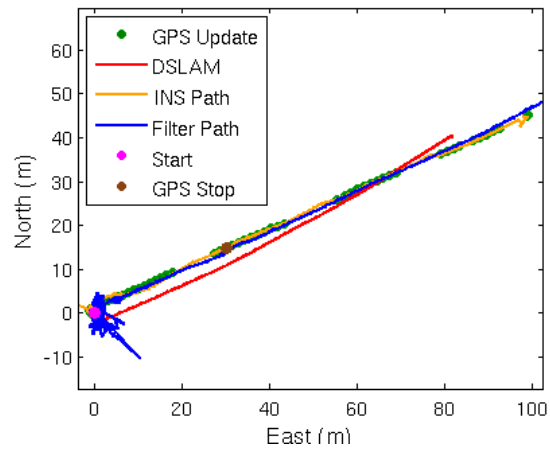


Fig. 3: Navigation results from the stereo vision (DSLAM), inertial (INS), and unified (Filter) navigation systems for a straight-line trajectory. The unified system accepts GPS updates for self-calibration during the first segment of the trajectory, then GPS updates are turned off and used only for comparison. The unified filter reduces drift in both the IMU and vision systems.

GPS, improving both the accuracy and usability of the IMU measurements. Fig. 5 shows the comparative performance of the IMU being updated by GPS versus by the vision system. Near the start of this path (at the left of the figure), the INS system's heading is inaccurate. The filter requires several GPS updates to correct the error, which is ultimately over-corrected for, leaving the IMU drifting in the opposite direction. The unified trajectory (comprising of vision and IMU updates) is updated more frequently, resulting in a significant reduction in the effects of IMU drift through more rapid and accurate corrections.

### 4.2. IMU Bias Estimation

The IMU rapidly drifts when unconstrained. This effect can be reduced by estimating the biases of the IMU using an EKF, which typically requires 30 to 60 seconds worth of data for this system, and removing them. The EKF in the INS system estimates these IMU biases using updates from the GPS receiver, which provides a 3 degree-of-freedom (DOF) position-only update at approximately 1 Hz. From the combination of these position updates and the measurement of the gravity vector, the system has sufficient observability into only 5 of the 6 total DOFs of the IMU. The EKF has limited observability of the Z-axis (yaw) gyro bias, as gravity does not typically project into this rotation axis in these operational scenarios.

Because DSLAM updates the filter more frequently, more precisely, and with all 6 DOFs, the unified system converges upon the IMU biases more rapidly and accurately than it does with GPS updates alone. DSLAM outputs a full 6-DOF navigation state at 20 Hz, is especially precise when the camera is stationary, and requires no initial calibration period. For this reason, the sensors are kept com-

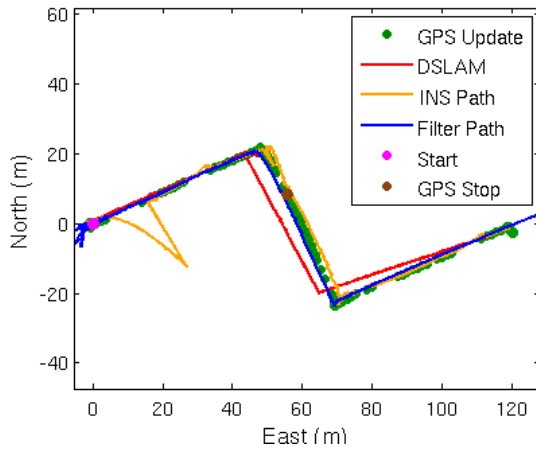


Fig. 4: Navigation results from the stereo vision (DSLAM), inertial (INS), and unified (Filter) navigation systems. The unified system is successfully able to navigate the 90-degree corner without GPS updates, which were turned off after the first corner. The inertial-only system drifts significantly during the loss of GPS near the beginning of the trajectory, but the vision updates keep the unified system from exhibiting this same behavior.

pletely stationary for the first 120 seconds of any dataset in order to collect particularly high precision vision data, which speeds up the IMU bias estimation by the filter. Fig. 6 shows the EKF gyro bias estimates over time for the same IMU measurements processed with and without vision updates. Not only does the addition of vision data allow proper estimation of the Z-axis gyro bias, but it also speeds up bias convergence for the X- and Y-axes. This allows the filter to use the IMU more effectively, improving the navigation performance of the unified system.

### 4.3. Rotation Rates

Rapid rotations result in errors in the vision system because the tracked features are too rapidly lost outside of the field of view of the camera. A well-constrained IMU can detect these rotation rates and help the system either maintain or regain its pose estimate after features are lost or as features are rapidly exiting the field of view, as long as the high-rate motion is brief in duration. In the unified inertial and vision navigation system, the vision system can provide accurate updates to the IMU until the high-rate motion begins, and quickly re-constrain the system again afterwards. As shown in Fig. 7, this results in improved accuracy when traversing sharp corners.

### 4.4. Vision System Dropouts

The worst errors in the vision system occur when all features are lost from the camera field of view, causing the vision system to stop returning motion estimates (often called a “dropout”). This happens mainly in low-

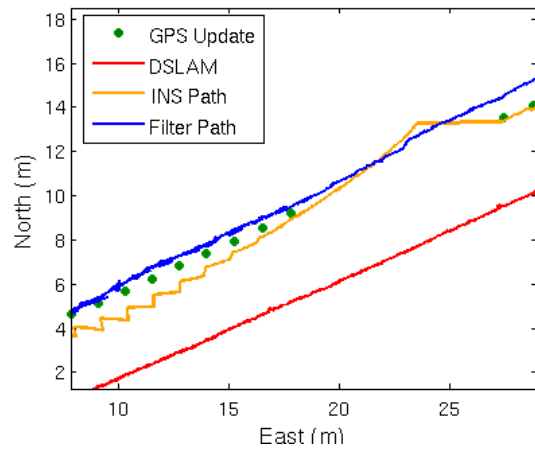


Fig. 5: The effect of IMU drift when updated using low-rate GPS (orange) versus high-rate vision (blue) updates. The frequent updates from the vision system result in a significant improvement in positioning accuracy.

contrast environments or due to lighting effects, such as lens flares. During these brief outages, the inertial system can continue to propagate the filter, allowing continued output of a navigation state estimate. Fig. 8a shows an example of a simulated 5 second vision dropout during a straight traverse, and Fig. 8b shows a simulated 10 second vision dropout during a gentle curve. Running independently, DSLAM halts motion entirely when it cannot detect enough features to calculate a camera pose estimate, and the INS would typically begin to rapidly drift (note that in these figures the INS is still being constrained by GPS updates, in order to better depict the behavior of the IMU during that time). When running with the combined filter, the IMU bias and drift are better accounted for, allowing the system to continue to navigate during brief periods of complete outage by both the vision and GPS systems.

## 5. SYSTEM TESTING

The Stingray navigation testbed was used to test the navigation performance of the DSLAM stereo vision navigation system and the unified inertial and vision navigation system in unstructured outdoor environments. An actual operational hopper was unavailable for testing, due to issues of availability and operational costs. For this reason, the system was designed to be portable and self-contained, making it operational in a variety of alternative contexts, including those of a pedestrian or a car. The experimental results presented here were selected for their similarities to various challenges a hopper navigation system must overcome. For example, while pedestrians move more slowly than hoppers, they have frequent, large disturbances and rapid rotations due to the dynamics of walking. A car has slower rotation rates and fewer disturbances, but velocities more comparable to those predicted of hoppers.

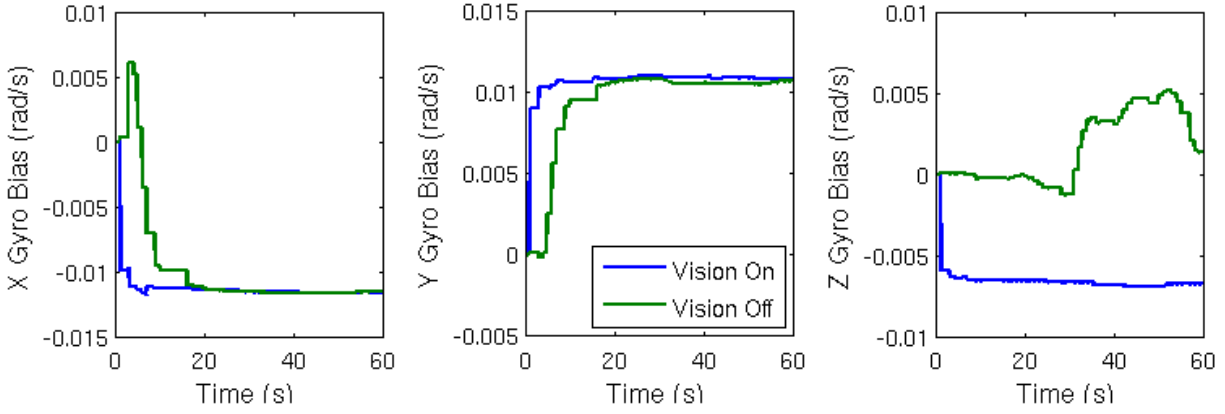


Fig. 6: Filter-calculated estimates of IMU gyro biases with and without vision updates. By incorporating vision updates, the filter gains visibility into the Z-axis gyro bias and is able to more rapidly converge upon the biases of all three gyros.

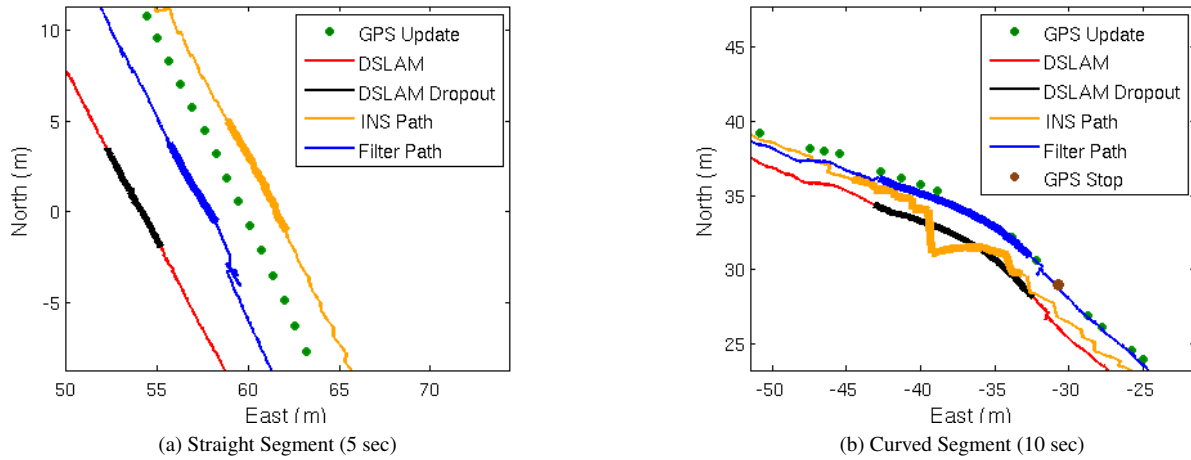


Fig. 8: Simulated vision system dropouts during a straight (left) and gently curved (right) trajectory. The unified system (in blue) is able to successfully navigate for brief periods in the absence of vision or GPS updates, making the system more robust to inconsistencies and changes in its operational environment. The affected segments are plotted in bold for emphasis. Note that the INS path still uses GPS updates here to constrain its error growth.

The results and discussion of system performance presented in this paper are based on three datasets selected for their ability to address the challenges of hopper navigation described in [2]. These datasets are discussed based on the operational settings of walking in natural environments and driving in urban environments. Discussion of additional datasets in the context of planetary hopping is available in [3].

### 5.1. Walking in Natural Environments

Two of the presented datasets were collected while walking outdoors at Halibut Point State Park, near Rockport, Massachusetts. The first route, referred to as “Halibut-Trail” and shown in Fig. 9, followed a hiking trail through the park for 790 meters. The hiking trail included natural terrain ranging from an open field to a forest, with several gentle curves.

The second route, referred to as “Halibut-Shore” and shown in Fig. 10, followed the rocky Atlantic shoreline for 180 meters at low tide. The only terrain visible in this dataset was large rocks, and the trajectory included several large disturbances and unsteady motion due to the uneven terrain being traversed by foot.

### 5.2. Driving in Urban Environments

The third presented dataset, referred to as “Cambridgeport” and shown in Fig. 11, was collected while driving 3.6 km through an urban residential area of Cambridge, Massachusetts. This route included three laps around a single block with only right turns followed by three laps around an adjacent block with only left turns, for a total of 28 corners, starting and ending at the same location. This makes it useful for evaluating cornering performance and consistency. This route also had the highest velocities of those presented, ranging from 7-9 m/s.

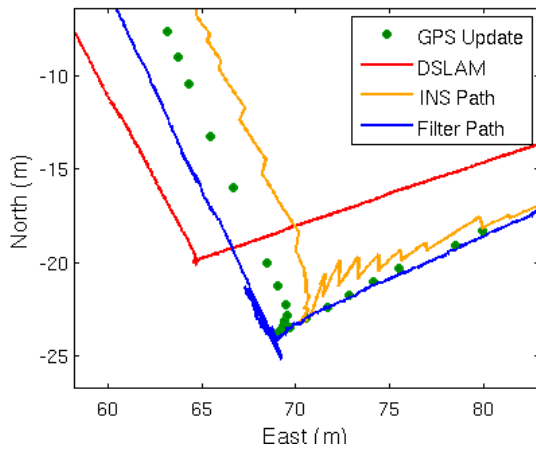


Fig. 7: The unified navigation filter improves performance during short periods of high-rate motion, such as sharp corners. DSLAM measures the corner to be  $98^\circ$ , while the unified system (shown with GPS updates turned off) measures it correctly as  $90^\circ$ . GPS updates are shown for reference but were not used by the unified filter.



Fig. 9: Typical terrain for the Halibut-Trail dataset, which involved walking on a wooded hiking trail.

### 5.3. Quantifying Error

A metric was used to objectively assess and compare the positional accuracy of calculated trajectories. This metric, called the Error Vector Sum (EVS) metric, is a measure of the similarity between two 3-dimensional paths of points [3]. It can be used to summarize system performance into a single numerical value, which can then be used to compare navigational performance of multiple trajectories. The EVS is not a perfect, all-encompassing measure of system performance, but it can be a useful tool for comparing navigation solutions.

The EVS metric is the sum of incremental errors of a measured trajectory with respect to some reference, normalized by the total distance traveled, as measured by the reference. A detailed derivation is available in [3]. With relative navigation systems, a small heading error early in a trajectory can appear as a much larger error late in the



Fig. 10: Typical terrain for the Halibut-Shore dataset, which involved walking on rocky terrain.



Fig. 11: Typical terrain for the Cambridgeport dataset, which involved driving in a residential neighborhood.

trajectory. This means that if error is calculated simply as the distance from a particular point to truth, errors occurring early in a trajectory would be weighted significantly higher than those occurring later in a trajectory. The EVS metric eliminates this problem by first removing the influence of previous measurements in the navigation system, and then calculating the error only for only a specific increment of the trajectory.

## 6. WALKING TESTS

The Halibut-Trail and Halibut-Shore datasets described above involved walking outdoors in a natural environment. These datasets were processed using both the vision-only and unified inertial and vision systems. The EVS metrics calculated for the DSLAM and filter trajectories are shown in Table 1.

### 6.1. Halibut-Trail Dataset

Fig. 12 shows both the vision-only and unified filter trajectories, as well as GPS reference data, for the Halibut-Trail dataset. GPS updates were used by the filter for cal-

Trajectory	Halibut-Trail	Halibut-Shore	Cambridgeport
DSLAM	0.248	0.241	0.243
Unified filter	0.296	0.338	0.163

Table 1: DSLAM and unified filter error metrics for walking and driving trajectories.

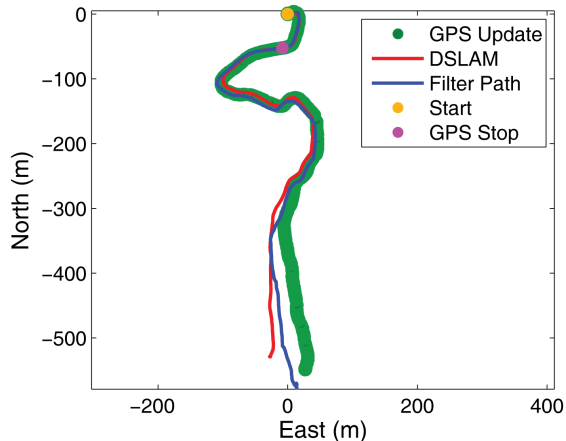


Fig. 12: DSLAM and unified filter-calculated trajectories for the Halibut-Trail dataset, which was collected while walking on a wooded hiking trail.

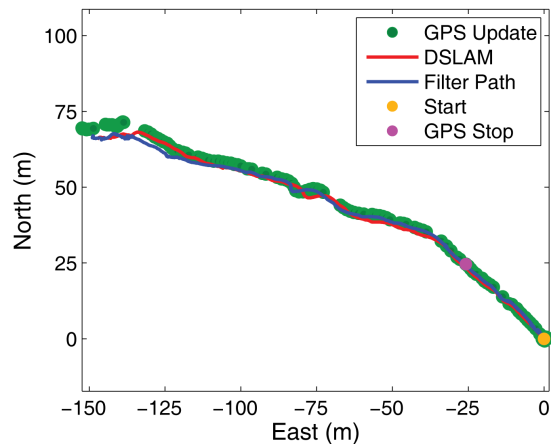


Fig. 13: DSLAM and unified filter-calculated trajectories for the Halibut-Shore dataset, which was collected while walking on rocky terrain.

ibration during the first 83 meters (10%) of the trajectory. In the figures, the magenta “GPS Stop” marker indicates where GPS was disabled. Near the last curve of both trajectories, a particularly large error was caused by camera glare, causing the only major divergence. Prior to that point, the system successfully navigated several difficult situations, such as brief vision outages and curves well over 90-degrees.

## 6.2. Halibut-Shore Dataset

Fig. 13 shows both the vision-only and unified filter trajectories, as well as GPS reference data, for the Halibut-Shore dataset. GPS updates were used for additional calibration during the first 36 m (20%) of the filter trajectory. As shown in the trajectory plot in Fig. 13, DSLAM and the unified filter were both very successful at navigating this terrain.

For this dataset, both the vision-only and filter trajectories were accurate to within a few meters at all times. This accuracy is partly due to the rocky features being perfectly stationary (unlike trees or grass, which often have small motions due to wind that cause measurement noise). The rocky terrain provided an abundance of high-contrast features which were guaranteed not to move, allowing accurate matching of features to existing landmarks within the map.

## 7. DRIVING TESTS

Fig. 14 shows both the vision-only and unified filter trajectories, as well as GPS reference data, for the Cambridgeport dataset. The initial calibration included GPS updates for the first 275 m (7.5%) of the trajectory and a full 360-degree circle while in GPS coverage to help calibrate the inertial sensor. The EVS metrics for this dataset are given in Table 1.

For the driving tests, the camera and IMU were fixed rigidly to the windshield of a passenger car. This led to smooth motions of the camera and less “noise” in the IMU compared to the dynamics of walking and holding the camera unsteadily. This resulted in the IMU being more reliable for the Cambridgeport dataset than either of the Halibut datasets.

### 7.1. Navigation Performance

Due to the improved IMU accuracy when collecting data using the car, the threshold for vision frame acceptance by the unified filter could be set especially high, meaning vision updates with higher effective uncertainties were not used. The DSLAM and filter trajectories register errors in different locations, indicating that the filter is successfully rejecting the majority of the erroneous vision frames, improving the accuracy of the filter.

Especially with the unified navigation filter, the system exhibited consistent performance while navigating re-

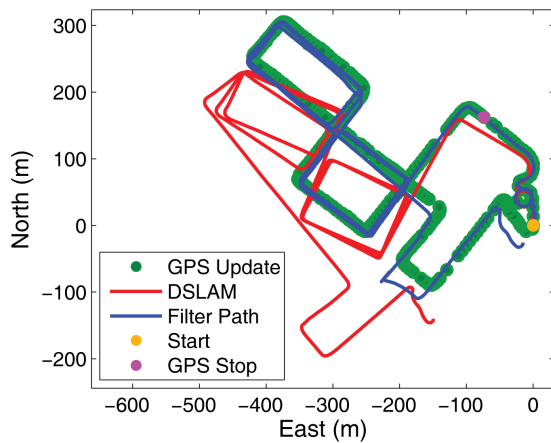


Fig. 14: DSLAM and unified filter-calculated trajectories for the Cambridgeport dataset, which was collected while driving in an urban environment.

peated turns and moderate velocities. These motions are more consistent with those planned for hoppers, with expected velocities in the range of 5-20 m/s, despite occurring in a different environment and operational context. These tests demonstrate that the navigation system is capable of accurately navigating within this range of motion, which is an important step toward preparing for a future flight demonstration of the system.

## 7.2. Elevation Profiles

Fig. 15a shows the calculated elevation profiles for the Cambridgeport trajectories, where the filter received a bad altitude calibration from GPS. The system was stationary for the first 120 seconds, and then the calibration loop, which was conducted on a level surface, was completed after about 200 seconds. This means the sensors are known to have remained at a very nearly constant altitude during this time, although GPS is shown to be drifting downward erroneously. This inaccurate GPS drift causes the Z-axis accelerometer to become incorrectly calibrated, leading to the system steadily drifting downward throughout the trajectory.

Fig. 15b shows the elevation profile of the same trajectory calculated using additional altitude updates from the barometric altimeter on the IMU interface board. Including even these uncertain altitude updates significantly improves the accuracy of the navigation filter. Although barometric altimetry is unavailable on airless bodies such as the Moon, a laser altimeter could provide similar updates at higher precision, constraining altitude drift.

## 8. CONCLUSIONS & FUTURE WORK

The testbed system produces promising results, especially given its early stage of development. Even when

using the low-grade sensors intended for preliminary development, the system does a very good job of navigating demonstration trajectories in a variety of environments. The effects of many of the observed current performance issues could be mitigated by upgrading the IMU to a model more likely to fly onboard a planetary exploration mission.

Section 6 presented results of tests conducted walking in outdoor environments. Walking on uneven terrain caused large disturbances, but the system was able to navigate the majority of these situations with reasonable accuracy (less than 5% final positioning error with respect to distance traveled). This suggests that the navigation system may be capable of handling moderate disturbances comparable to those experienced by a hopper.

Section 7 presented results of tests conducted while driving in an urban environment, where the system successfully navigated repeated corners and moderate velocities throughout the test run. The unified system did especially well in these tests, due to the smoother dynamics of the car as opposed to the pedestrian, achieving navigation accuracies of less than 1% error in final position with respect to total distance traveled. This suggests that if the vehicle dynamics of a hopper can be kept fairly steady, navigation of long-distance hops in moderately feature-rich environments is feasible.

The success of the various testbed demonstrations establish the system at NASA Technology Readiness Level (TRL) 4\*, and supports additional development of the system. This will involve re-testing the system with more accurate truth data to better determine performance limitations and integrating the system with a flight vehicle for open-loop flight tests, advancing the system to TRL 5<sup>†</sup>. Possible future closed-loop testing onboard a terrestrial rocket would further advance the system to TRL 6<sup>‡</sup>, enabling selection of the system by a flight program.

## REFERENCES

1. P. M. Cunio, F. Alibay, P. Meira, T. Sheerin, E. Lanford, E. Krupczak, and J. A. Hoffman, "Options in the solar system for planetary surface exploration via hopping," in *Proceedings of the 2011 IEEE Aerospace Conference*, Big Sky, Montana, March 5 - 12, 2011.
2. T. J. Steiner, S. A. Rasmussen, P. A. DeBitetto, B. E. Cohanin, and J. A. Hoffman, "Unifying inertial and relative solutions for planetary surface navigation," in *Proceedings of the 2012 IEEE Aerospace Conference*, Big Sky, Montana, March 3-10, 2012.

\*The Technology Readiness Level (TRL) is a metric used by NASA to evaluate the maturity of a technology. TRL 4 is defined as "Component and/or breadboard validation in laboratory environment" [17].

<sup>†</sup>"Component and/or breadboard validation in relevant environment" [17].

<sup>‡</sup>"System/subsystem model or prototype demonstration in a relevant environment (ground or space)" [17].

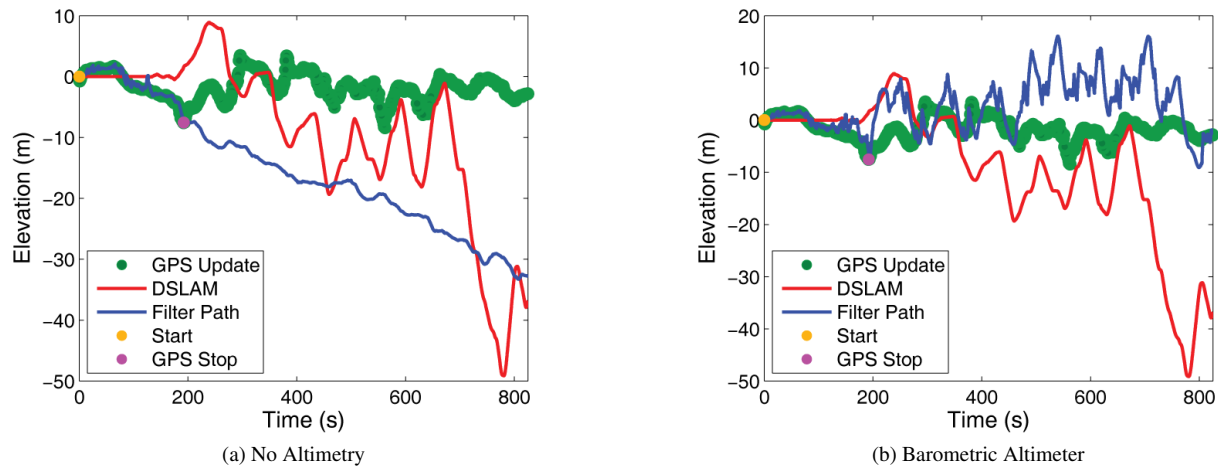


Fig. 15: DSLAM and unified filter-calculated elevation profiles for the Cambridgeport dataset, calculated with and without the onboard barometric altimeter. Use of additional altimeter data helps to reduce elevation drift.

3. T. J. Steiner, "A unified vision and inertial navigation system for planetary hoppers," Master's thesis, Massachusetts Institute of Technology, 2012.
4. S. Paschall and T. Brady, "Demonstration of a safe & precise planetary landing system on-board a terrestrial rocket," in *Proceedings of the 2012 IEEE Aerospace Conference*, Big Sky, Montana, March 3-10, 2012.
5. C. Rossi, P. M. Cunio, F. Alibay, J. Morrow, S. L. Nothnagel, T. Steiner, C. J. Han, E. Lanford, and J. A. Hoffman, "TALARIS Project update: Overview of flight testing and development of a prototype planetary surface exploration hopper," in *Proceedings of the 62nd International Astronautical Congress*, Cape Town, South Africa, 2011.
6. D. Adams, T. B. Criss, and U. J. Shankar, "Passive optical terrain relative navigation using APLNav," in *Proceedings of the 2008 IEEE Aerospace Conference*, Big Sky, Montana, March 1-8, 2008.
7. A. I. Mourikis, N. Trawny, S. I. Roumeliotis, A. E. Johnson, A. Ansar, and L. Matthies, "Vision-aided inertial navigation for spacecraft entry, descent, and landing," *IEEE Transactions on Robotics*, vol. 25, no. 2, pp. 264–280, 2009.
8. G. Flandin, B. Polle, J. Lheritier, and P. Vidal, "Vision based navigation for autonomous space exploration," in *Proceedings of the 2010 NASA/ESA Conference on Adaptive Hardware and Systems*, 2010.
9. L. Singh and S. Lim, "On lunar on-orbit vision-based navigation: Terrain mapping, feature tracking driven EKF," in *Proceedings of the AIAA Guidance, Navigation and Control Conference*, Honolulu, Hawaii, 2008.
10. P. Corke, "An inertial and visual sensing system for a small autonomous helicopter," *Journal of Robotic Systems*, vol. 21, no. 2, pp. 43–51, 2004.
11. R. Madison, G. Andrews, P. Debitetto, S. Rasmussen, and M. Bottkol, "Vision-aided navigation for small UAVs in GPS-challenged environments," in *2007 AIAA InfoTech at Aerospace Conference*, vol. 3, Rohnert Park, CA, May 7 - 10, 2007, pp. 2733–2745.
12. A. D. Wu and E. N. Johnson, "Autonomous flight in GPS-denied environments using monocular vision and inertial sensors," in *AIAA Infotech at Aerospace*, Atlanta, Georgia, April 20-22, 2010.
13. M. Achtelik, M. Achtelik, S. Weiss, and R. Siegwart, "Onboard IMU and monocular vision based control for MAVs in unknown in- and outdoor environments," in *IEEE International Conference on Robotics and Automation*, Piscataway, New Jersey, May 9-13, 2011, pp. 3056–63.
14. J. Wendel, O. Meister, C. Schlaile, and G. F. Trommer, "An integrated GPS/MEMS-IMU navigation system for an autonomous helicopter," *Aerospace Science and Technology*, vol. 10, no. 6, pp. 527–533, 2006.
15. S. Nassar, Z. Syed, X. Niu, and N. El-Sheimy, "Improving MEMS IMU/GPS systems for accurate land-based navigation applications," in *Proceedings of the 2006 National Technical Meeting of The Institute of Navigation*, vol. 1, Monterey, California, January 18-20, 2006, pp. 523–529.
16. C. Mei, G. Sibley, M. Cummins, P. Newman, and I. Reid, "RSLAM: a system for large-scale mapping in constant-time using stereo," *International Journal of Computer Vision*, vol. 94, no. 2, pp. 198–214, 2011.
17. S. J. Kapurch and N. E. Rainwater, *NASA Systems Engineering Handbook*. Washington, D.C.: National Aeronautics and Space Administration, 2007, pp. 296–297.